ARTICLE

New nickel(II) Schiff base complexes as potential tool against SARS-CoV-2 Omicron target proteins: An *in-silico* approach

Sunil Kumar[a], Mukesh Choudhary[a]*

[a] *Department of Chemistry, National Institute of Technology Patna, Patna-800005 (Bihar) India.*

[a.] **Corresponding author: mukesh@nitp.ac.in*

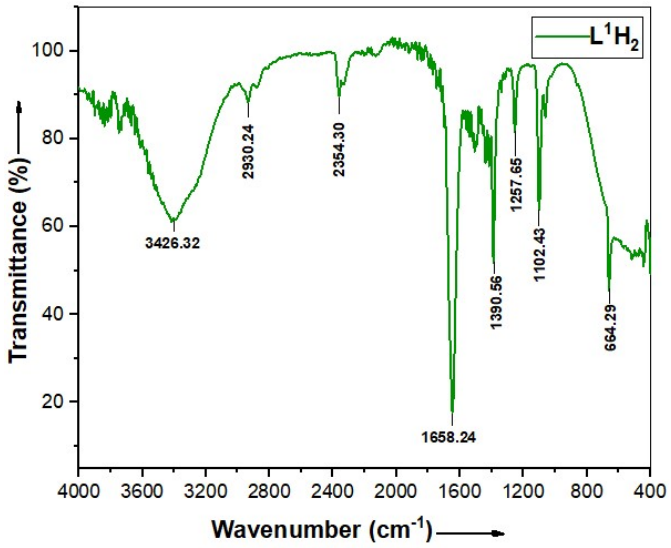

Figure S1. FT-IR spectra of Schiff base ligand L^1H_2.

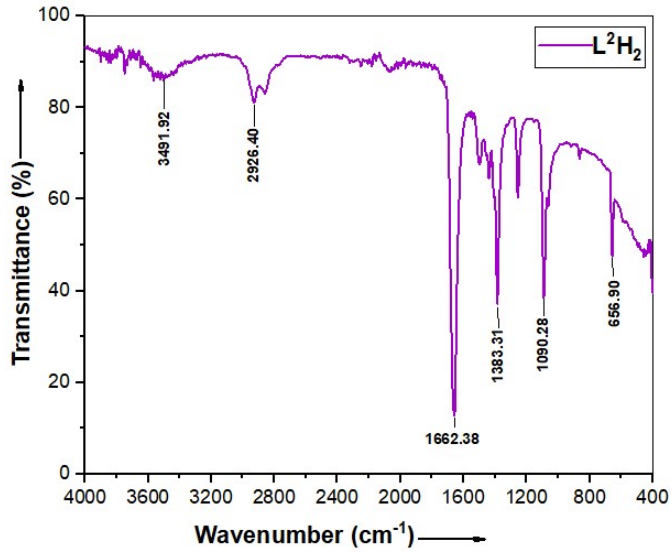

Figure S2. FT-IR spectra of Schiff base ligand L^2H_2.

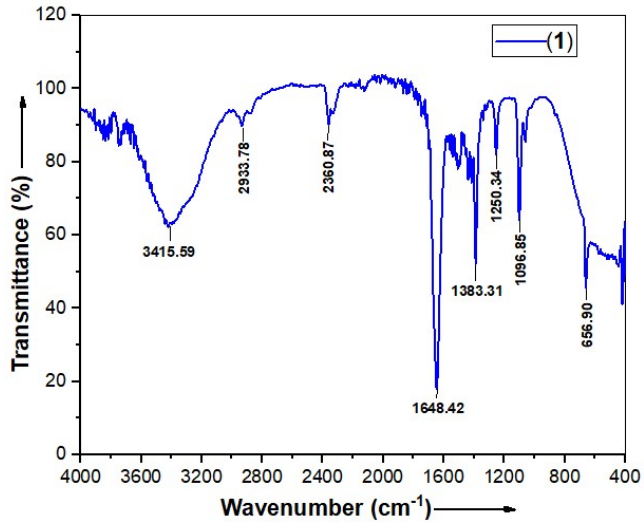

Figure S3. FT-IR spectra of nickel(II) complex $[Ni(L^1)](PPh_3)]DMF$(**1**) of L^1H_2.

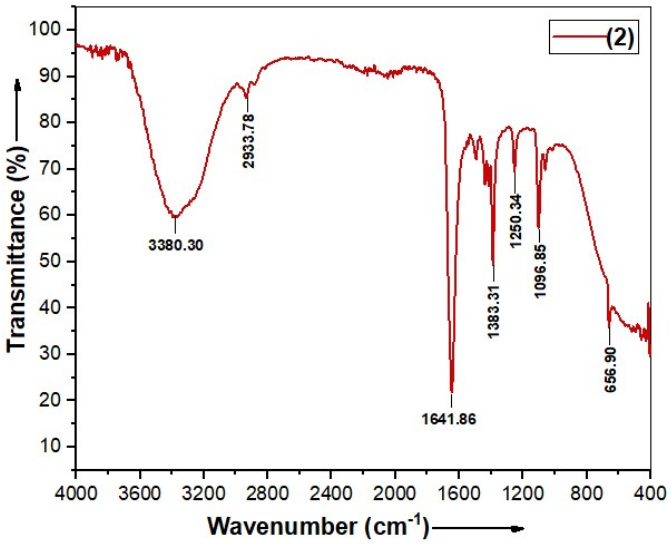

Figure S4. FT-IR spectra of nickel (II) complex$[Ni(L^2)]$(**2**) of L^2H_2.

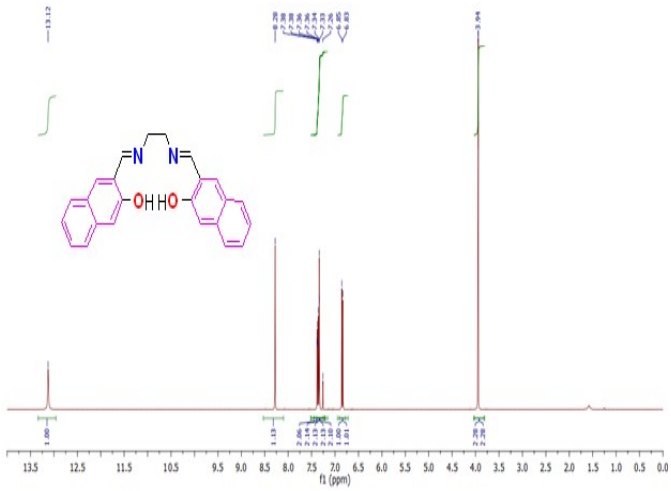

Figure S5. ^{1}H-NMR spectra of Schiff base ligand L^2H_2.

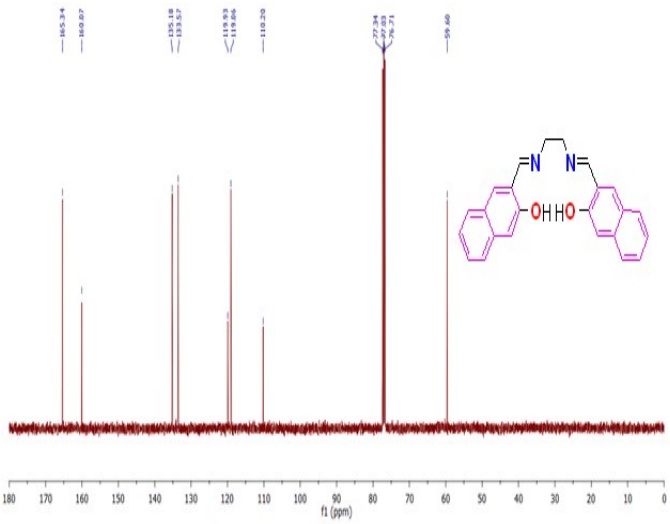

Figure S6. ^{13}C-NMR spectra of Schiff base ligand L^2H_2.

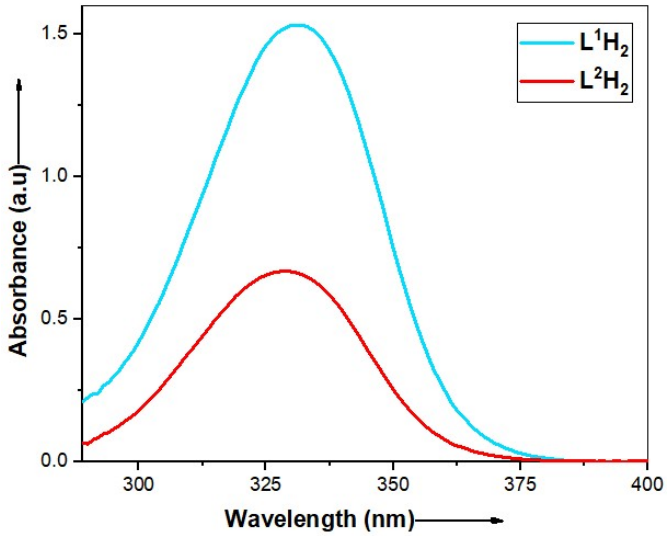

Figure S7. UV-Vis spectrum of Schiff base ligands (L^1H_2 and L^2H_2) in DMSO (3 x10^{-3} M) solvent at room temperature.

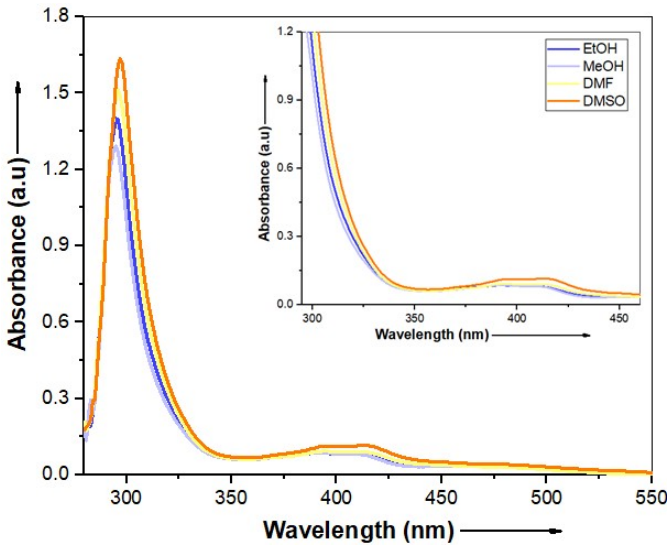

Figure S8. UV-Vis spectrum of nickel (II) complex [Ni(L^1)](PPh_3)]DMF (**1**) in different solvents (3 x 10^{-3} M) at room temperature.

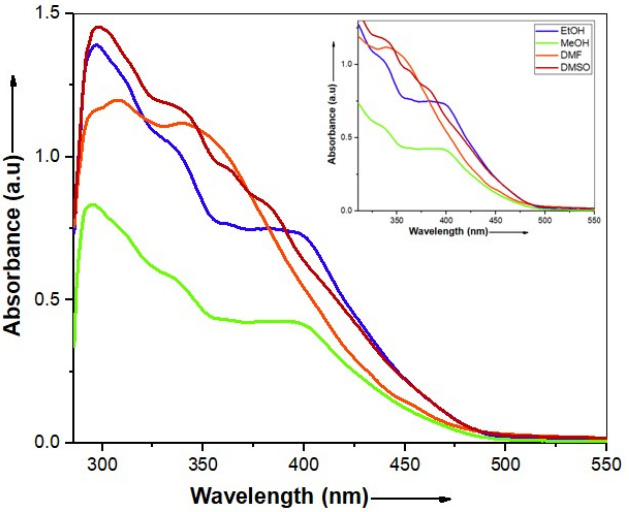

Figure S9. UV-Vis spectrum of nickel (II) complex [Ni(L^2)] (**2**) in different solvents (3 x 10^{-3} M) at room temperature.

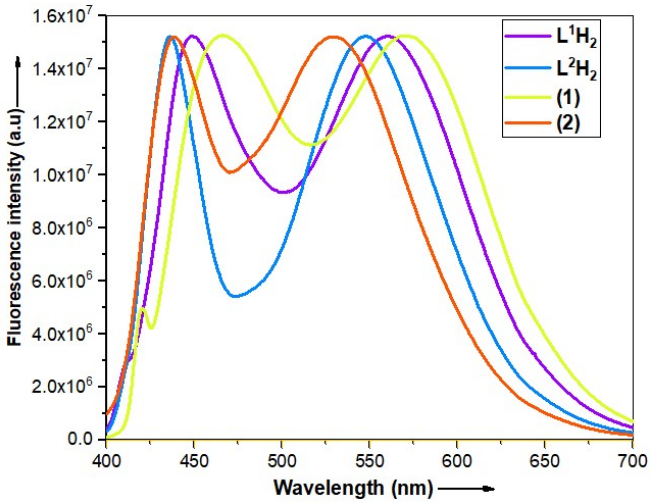

Figure S10. Fluorescence spectra of Schiff base ligands (L^1H_2/L^2H_2) and nickel complex [Ni(L^1)](PPh_3)DMF(**1**) and [Ni(L^2)](**2**) in EtOH (3x10^{-3} M) at room temperature.

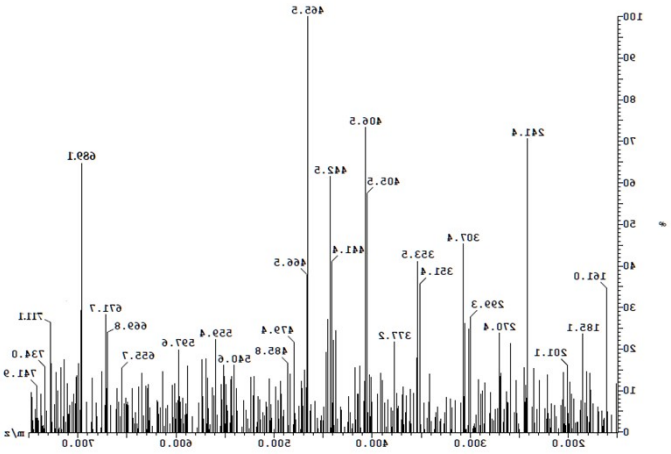

Figure S11. LC-MS spectra of Ni(II) complex [Ni(L^1)](PPh_3)]DMF(**1**).

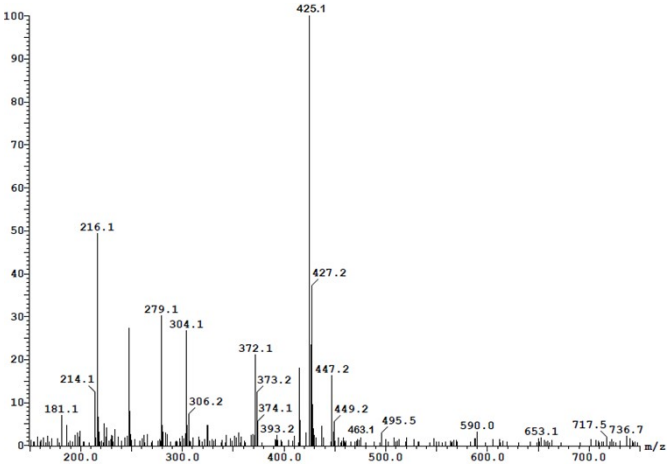

Figure S12. LC-MS spectra of Ni(II) complex [Ni(L^1)](**2**) .

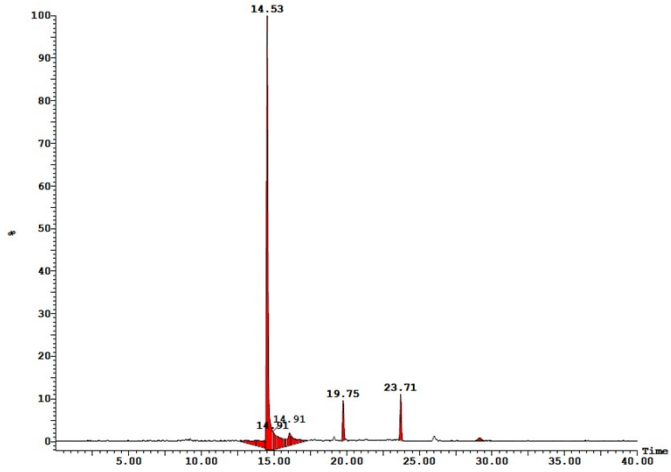

. **Figure S13.** Retention peak of Ni(II) complex [Ni(L^1)](PPh$_3$)]DMF(**1**).

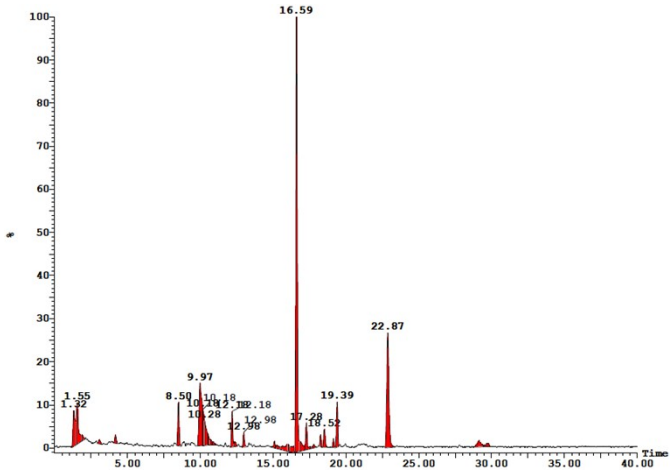

Figure S14. Retention peak of Ni(II) complex [Ni(L^1)](**2**).

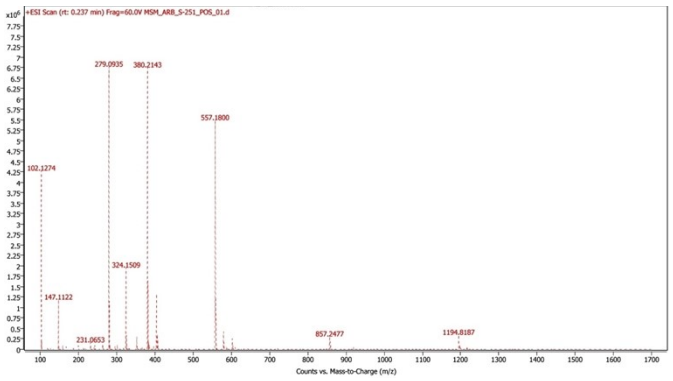

Figure S15. Mass spectra of Ni(II) complex [Ni(L^1)](PPh$_3$)]DMF(**1**).

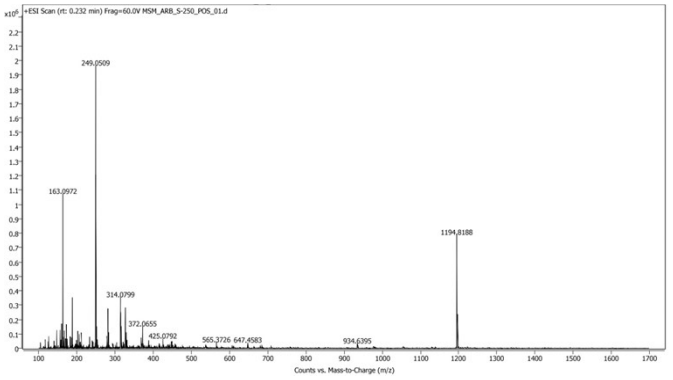

Figure S16. Mass spectra of Ni(II) complex [Ni(L^1)](**2**) .

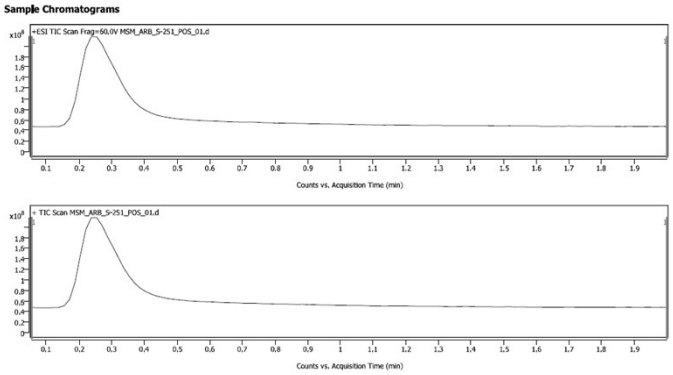

Figure S17. Scan rate of Ni(II) complex [Ni(L^1)](PPh$_3$)]DMF(**1**).

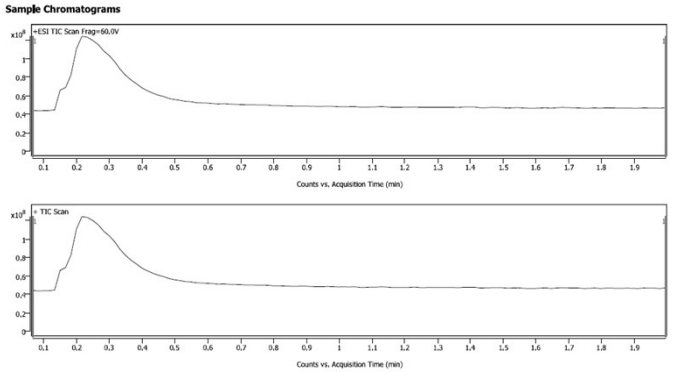

Figure S18. Scan rate of Ni(II) complex [Ni(L^1)](**2**).

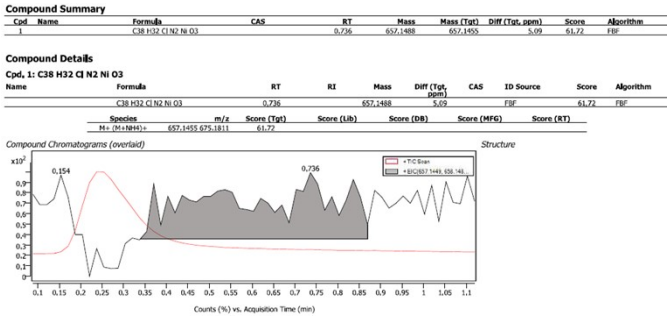

Figure S19. View of base peak chromatograms of Ni(II) complex [Ni(L^1)](PPh_3)]DMF(**1**).

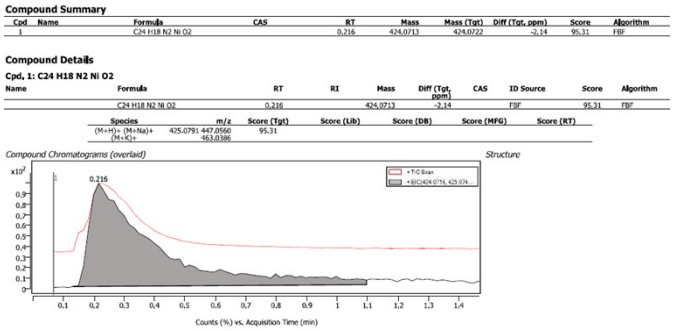

Figure S20. View of base peak chromatograms of Ni(II) complex [Ni(L^1)](**2**).

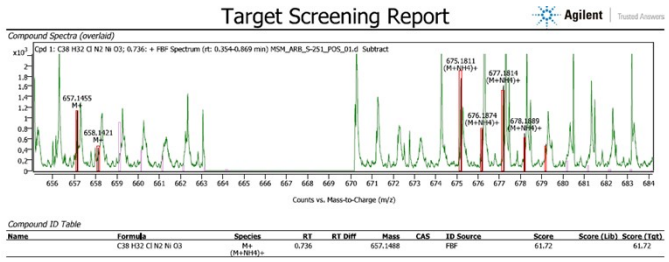

Figure S21. View of target screening report for Ni(II) complex [Ni(L^1)](PPh_3)]DMF(**1**).

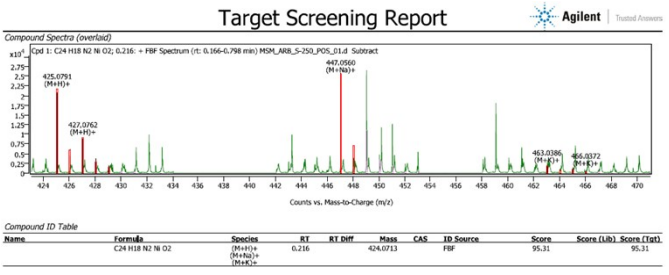

Figure S22. View of target screening report for Ni(II) complex [Ni(L^1)](**2**).

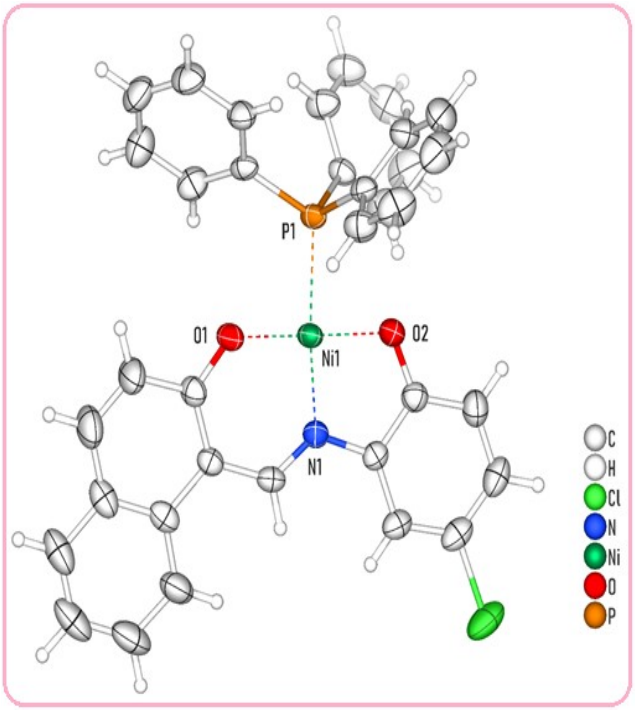

Figure S23. Shelx structure of the Ni(II) complex [Ni(L^1)(PPh_3)]DMF (**1**).

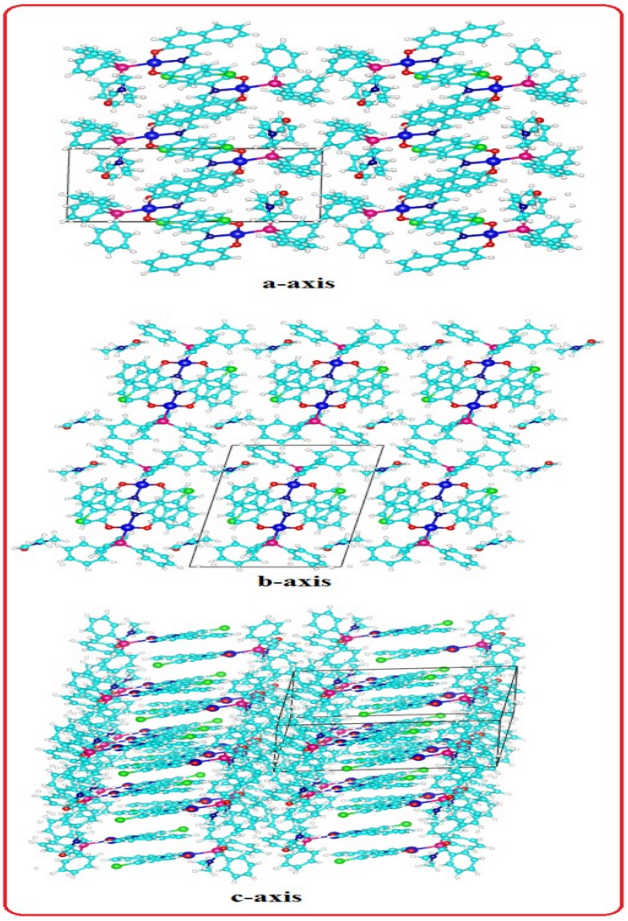

Figure S24: Packing view of Ni(II) complex [Ni(L^1)](PPh_3)]DMF (**1**) (along the *a*-*c*-axis).

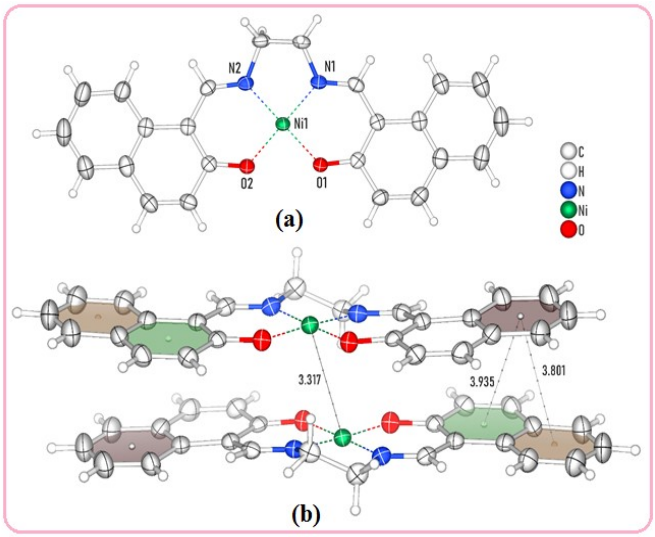

Figure S25. Shelx structure of the Ni(II) complex [Ni(L^2)](**2**) with (a) monomer and (b) dimer structure . The Ni...Ni separation is 3.317 Å in dimer Ni(II) complex (**2**).

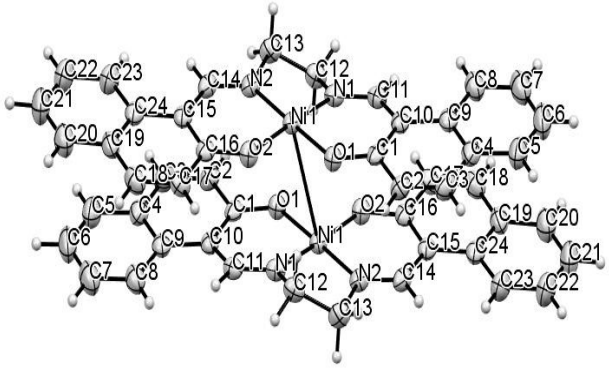

Figure S26. ORTEP representation of dimer Ni(II) complex [Ni(L^2)]$_2$(**2**); with thermal ellipsoids were drawn at 50 % probability level.

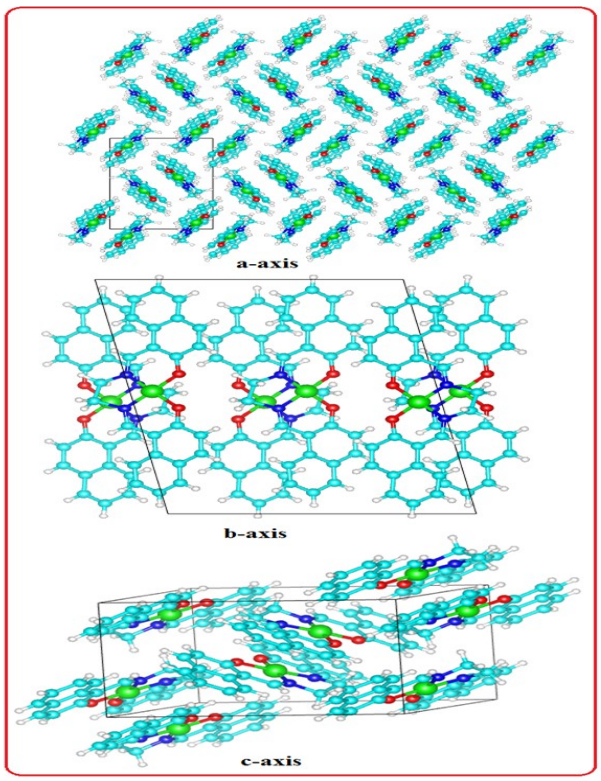

Figure S27. Packing view of the Ni(II) complex [Ni(L^2)](**2**) (along the *a*-*c*-axis).

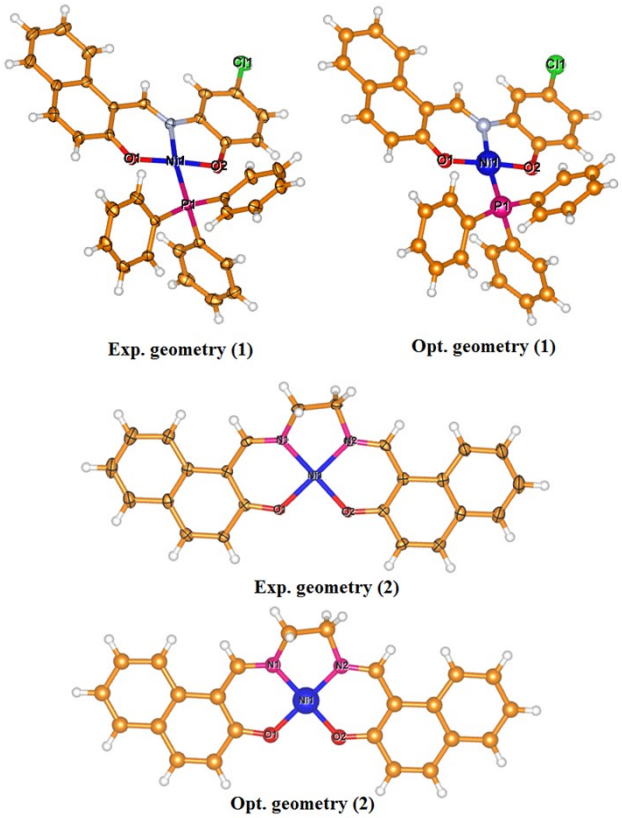

Figure S28. Optimized and experimental geometry of Ni(II) complex [Ni(L^1)](PPh$_3$)]DMF(**1**) of L^1H_2 and [Ni(L^2)](**2**) of L^2H_2.

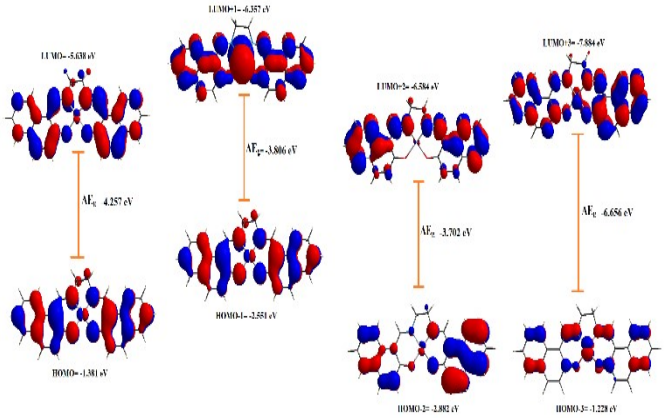

Figure S29. The atomic orbital composition of the frontier molecular orbitals of Ni(II) complex (**2**) of L^2H_2 .

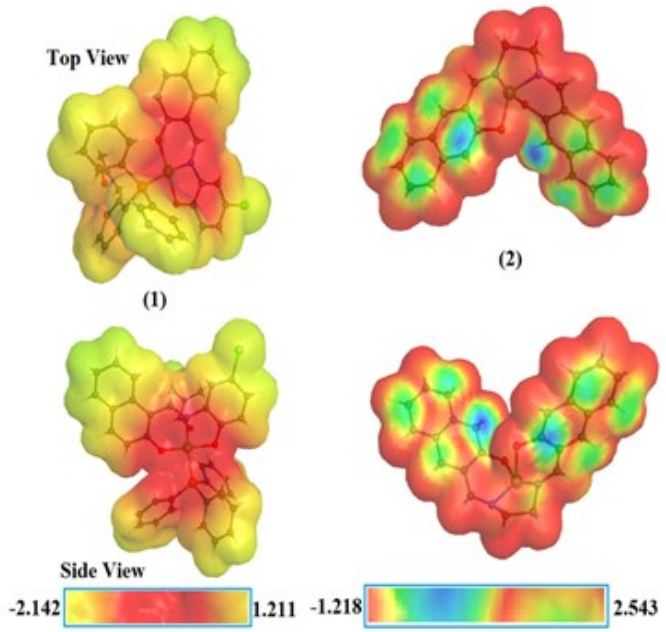

Figure S30. The molecular electrostatic potential maps (MEPs) of Ni(II) complex [Ni(L^1)](PPh$_3$)]DMF(**1**) of L^1H_2 and [Ni(L^2)] (**2**) of L^2H_2 with iso-value of 0.020 to 0.024 a.u., where negative potential decreases in order of red>orange>yellow>green>blue.

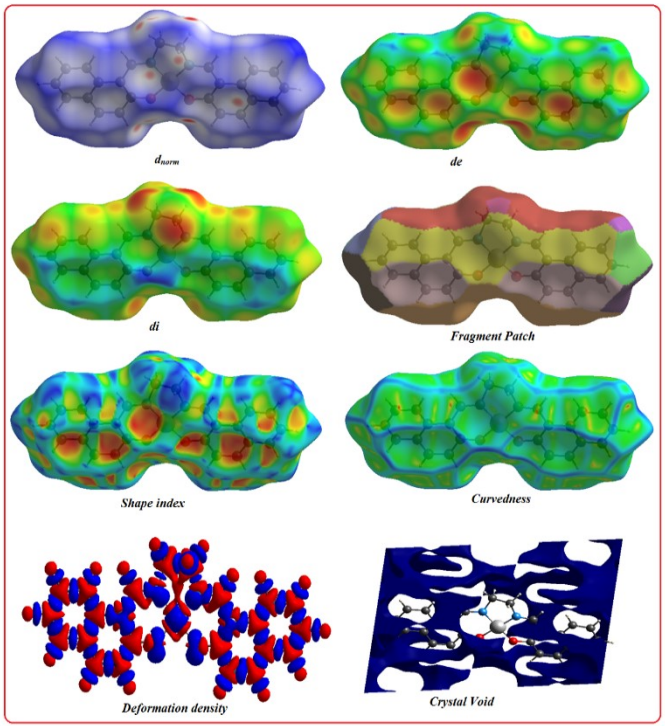

Figure S31. Graphical view of the Hirshfeld surfaces (HS) for Ni(II) complex [Ni(L^2)](**2**) mapped with d_{norm}, d_i, d_e, shape index, Fragment patch, curvedness, deformation density and crystal void; red spots represents the closest contacts and blue colour the most distant contacts for the Ni(I) complex (**2**).

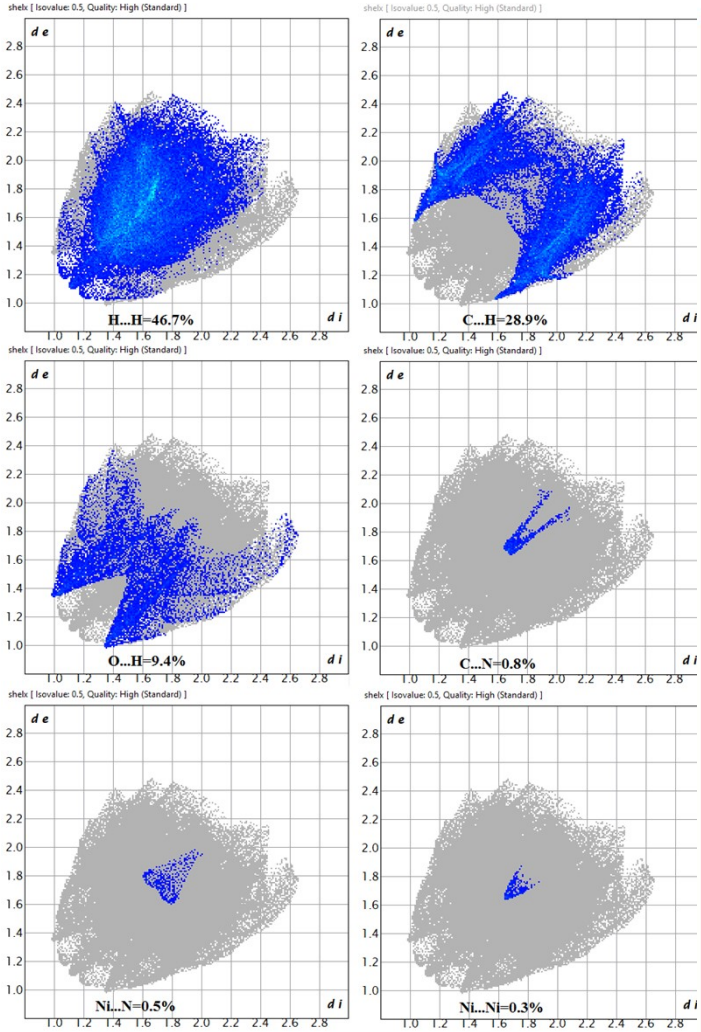

Figure S32. Graphical view with 2D Fingerprint plots of Ni(II) complex [Ni(L^2)](**2**) showing percentage of contacts contributed to the total Hirshfeld surface (HS) area of the molecules; d_i and d_e are the distances from the surface to the nearest atoms interior and exterior to the surface, respectively.

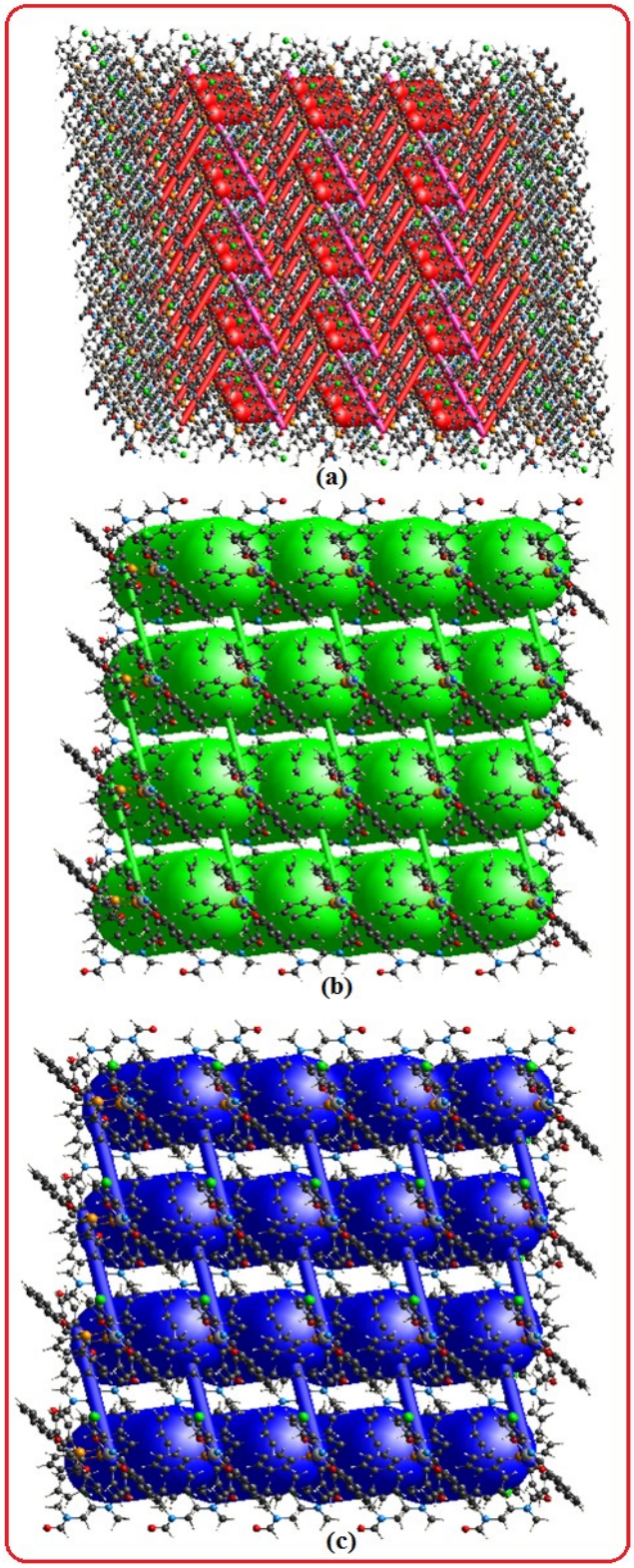

Figure S33. 3D graphical representation of energy framework diagrams for Ni(II) complex [Ni(L^2)] (**2**); (a) Dispersion energy (E_{dis}), (b) Coulomb energy (E_{coul}), (c) Total energy (E_{tot}) for cluster of molecule in Ni(II) complex (**2**). Hydrogen atoms have been omitted for clarity and all diagrams used the same cylindrical scale of 300 for energies.

Figure S34. Computed CE-B3LYP estimates of energy components and total energies (kJ/mol) for the closest intermolecular interactions of Ni(II) complex [Ni(L^1)](PPh_3)]DMF(**1**) and [Ni(L^2)] (**2**).

Complex (1)

	N	Symop	R	Electron Density	E_ele	E_pol	E_dis	E_rep	E_tot
	2	x, -y+1/2, z+1/2	18.00	HF/3-21G	2.0	-0.4	-7.1	0.0	-4.7
	2	x, y, z	17.87	HF/3-21G	-2.9	-0.5	-8.6	0.0	-11.0
	2	-x, y+1/2, -z+1/2	17.34	HF/3-21G	-0.1	-0.4	-6.1	0.0	-5.8
	1	-x, -y, -z	18.43	HF/3-21G	1.6	-0.1	-1.0	0.0	0.6
	2	-x, y+1/2, -z+1/2	6.12	HF/3-21G	-8.0	-5.5	-46.6	17.0	-40.0
	2	x, -y+1/2, z+1/2	6.70	HF/3-21G	-25.6	-11.8	-43.2	28.9	-49.3
	1	-x, -y, -z	3.52	HF/3-21G	-45.6	-30.0	-163.5	98.6	-133.3
	2	-x, y+1/2, -z+1/2	9.62	HF/3-21G	2.7	-0.9	-3.8	0.0	-1.2
	1	-x, -y, -z	6.00	HF/3-21G	-28.9	-8.9	-60.2	28.2	-66.5
	1	-x, -y, -z	18.64	HF/3-21G	-0.6	-0.2	-4.7	0.0	-4.9

Energy Model	k_ele	k_pol	k_disp	k_rep
CE-HF ... HF/3-21G electron densities	1.019	0.651	0.901	0.811
CE-B3LYP ... B3LYP/6-31G(d,p) electron densities	1.057	0.740	0.871	0.618

Complex (2)

	N	Symop	R	Electron Density	E_ele	E_pol	E_dis	E_rep	E_tot
	1	-x, -y, -z	18.45	HF/3-21G	0.7	-0.2	-5.0	0.0	-3.9
	2	x, -y+1/2, z+1/2	17.81	HF/3-21G	0.2	-0.4	-7.7	0.0	-7.0
	2	x, y, z	17.69	HF/3-21G	-0.1	-0.5	-9.3	0.0	-8.9
	2	-x, y+1/2, -z+1/2	6.06	HF/3-21G	-8.7	-5.5	-50.0	20.0	-41.4
	1	-x, -y, -z	3.48	HF/3-21G	-51.6	-31.1	-173.6	111.7	-138.7
	2	x, -y+1/2, z+1/2	6.63	HF/3-21G	-26.8	-12.2	-46.1	33.3	-49.7
	2	-x, y+1/2, -z+1/2	9.51	HF/3-21G	2.8	-1.0	-4.0	0.0	-1.4
	2	-x, y+1/2, -z+1/2	17.16	HF/3-21G	1.3	-0.4	-6.6	0.0	-4.9
	1	-x, -y, -z	5.93	HF/3-21G	-29.8	-9.3	-64.5	33.0	-67.8
	1	-x, -y, -z	18.24	HF/3-21G	2.0	-0.1	-1.1	0.0	1.0

Energy Model	k_ele	k_pol	k_disp	k_rep
CE-HF ... HF/3-21G electron densities	1.019	0.651	0.901	0.811
CE-B3LYP ... B3LYP/6-31G(d,p) electron densities	1.057	0.740	0.871	0.618

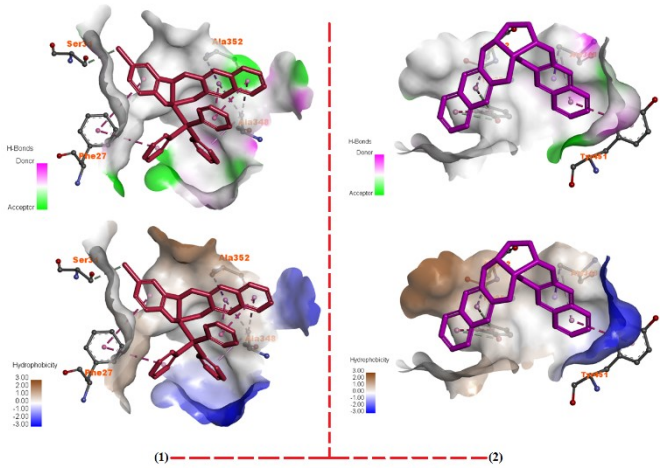

Figure S35. H-bond (top view) and hydrophobicity (bottom view) plot of interacting amino acid residues of SARS-CoV-2 spike protein (PDB ID: 7CWO) with the Ni(II) complex (**1**) and (**2**). The complexes are displayed in red and pink colour.

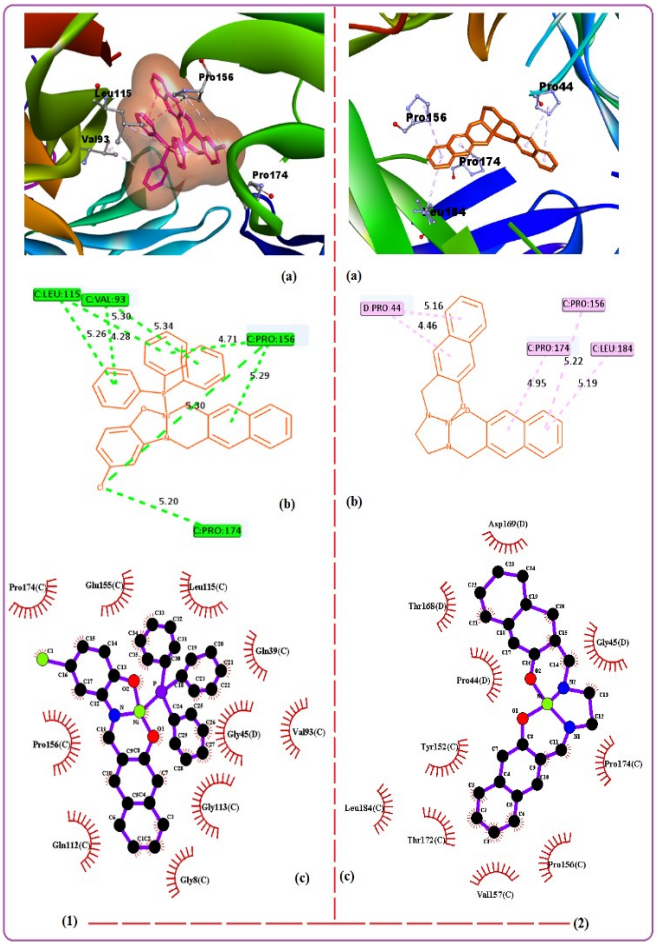

Figure S36. View of docked Ni(II) complex **(1)** and (**2**) with the binding cavity of the spike protein interaction of SARS-CoV-2 Omicron variant (PDB ID: 7WK8). The 2D interaction plot and Lig-Plot interaction of docked complexes with focussed for interacting different amino acid residues.

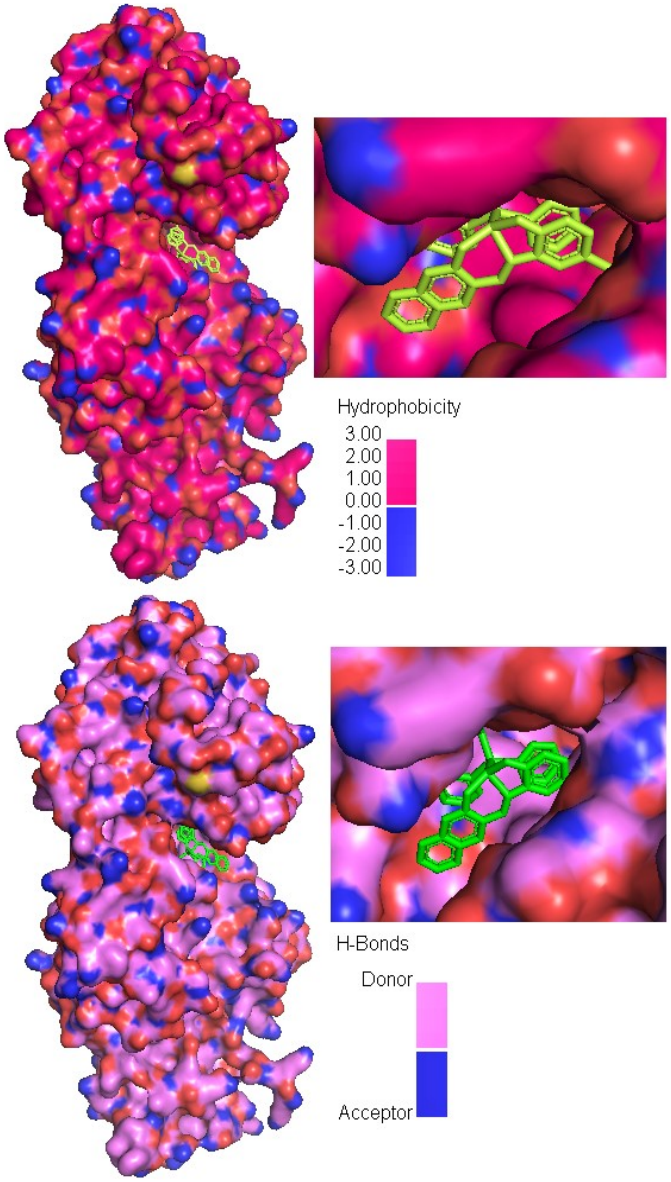

Figure S37. View of the total density surfaces representation for docked Ni(II) complex (**1**) inside the SARS-CoV-2 Omicron spike protein (PDB ID: 7WK8); hydrophobic pocket represented with deep pink and blue colours; hydrogen bond donor and acceptor meshes represented by light pink and dark navy blue colours, respectively.

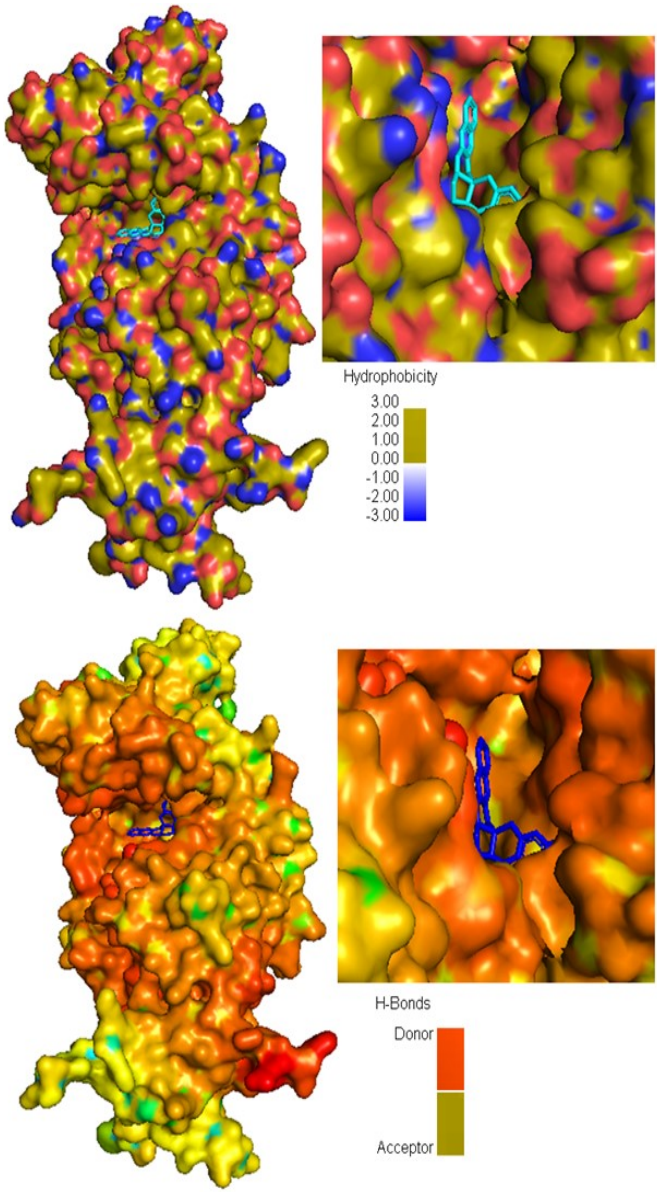

Figure S38. View of the total density surfaces representation for docked Ni(II)complex (**2**) inside the SARS-CoV-2 Omicron spike protein (PDB ID: 7WK8), hydrophobic pocket represented with deep yellow and blue colours; hydrogen bond donor and acceptor meshes represented by orange and light yellow colours, respectively.

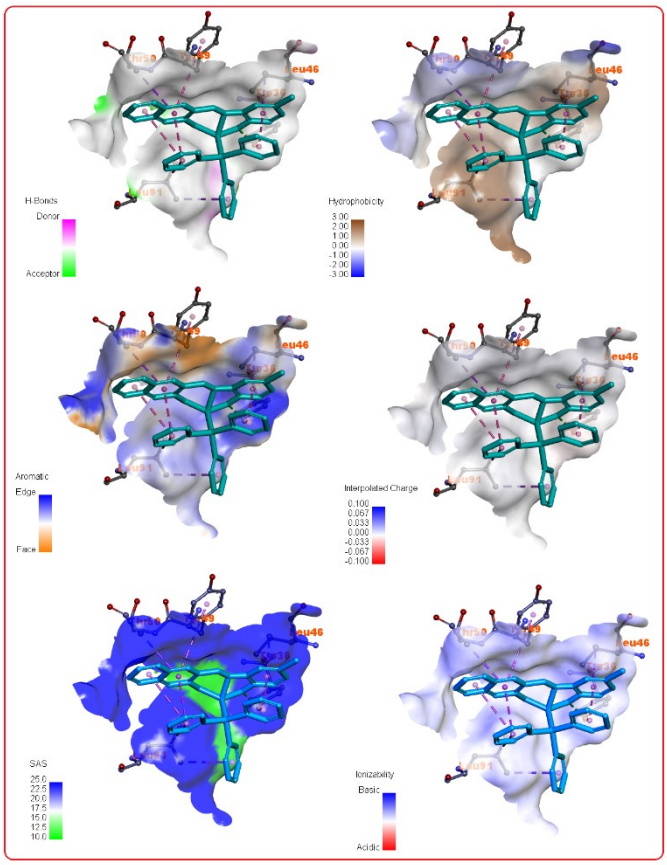

Figure S39. Graphical representation of docked Ni (II) complex (**1**) inside the SARS-CoV-2 Omicron spike protein (PDB ID: 7QTK) with its focused view for interacting residues along with H-bond and intermolecular interactions; (a) H-bond donor and acceptor meshes represented by pink and light green colours, respectively; (b) Hydrophobic pocket represented with blue and brown colours; (c) Aromatic receptor surface represented by blue (Edge) and light orange (face) colours; (d) interpolated charge receptor surface represented by blue and red colours; (e) SAS receptor surface represented by blue and light green colours, respectively; (f) ionizability receptor surface represented by blue (basic) and red (acidic) colours.

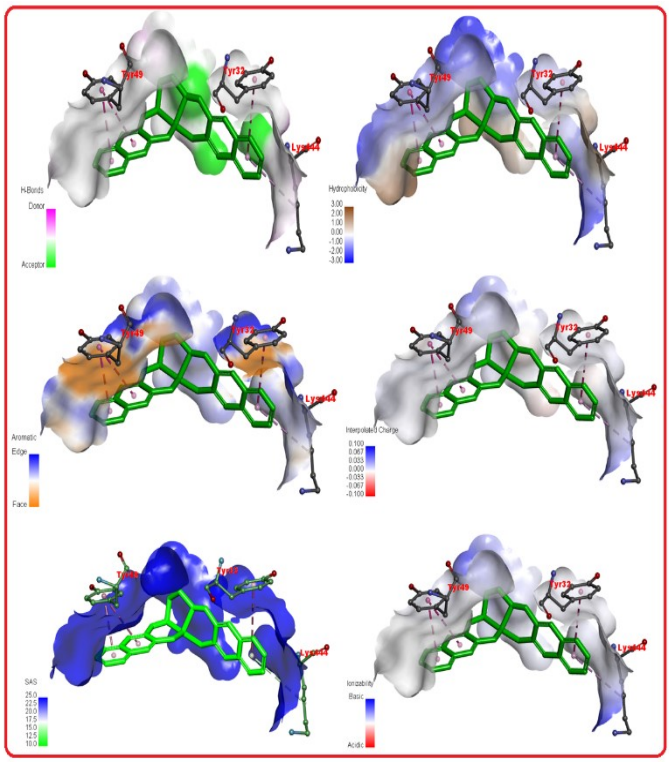

Figure S40. Graphical representation of docked Ni (II) complex (**2**) inside the SARS-CoV-2 Omicron spike protein (PDB ID: 7QTK) with its focused view for interacting residues along with H-bond and intermolecular interactions; (a) H-bond donor and acceptor meshes represented by pink and light green colours, respectively; (b) Hydrophobic pocket represented with blue and brown colours; (c) Aromatic receptor surface represented by blue (Edge) and light orange (face) colours; (d) interpolated charge receptor surface represented by blue and red colours; (e) SAS receptor surface represented by blue and light green colours, respectively; (f) ionizability receptor surface represented by blue (basic) and red (acidic) colours.

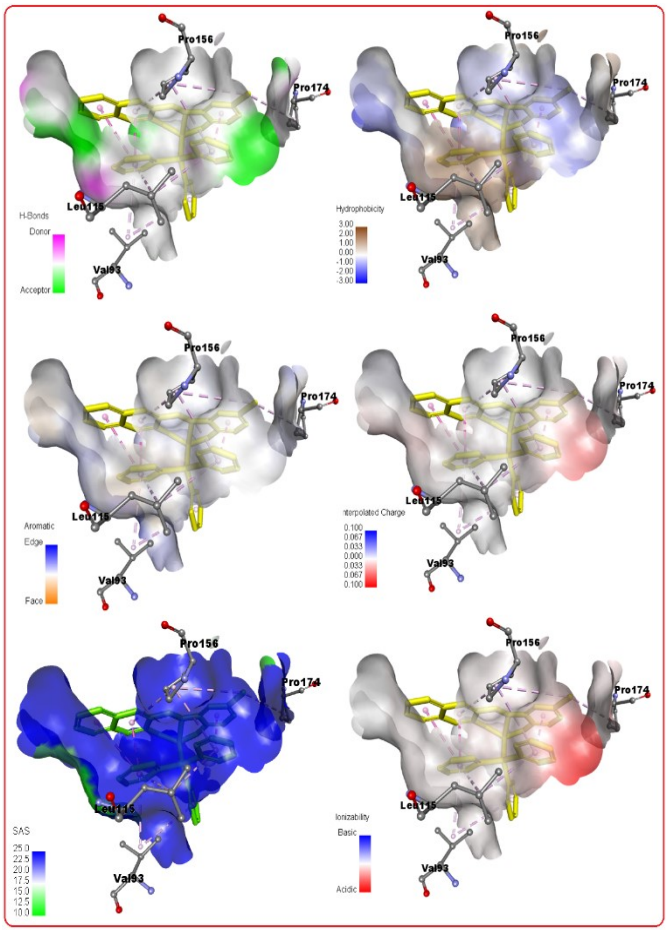

Figure S41. Graphical representation of docked Ni (II) complex (**1**) inside the SARS-CoV-2 Omicron spike protein (PDB ID: 7WK8) with its focused view for interacting residues along with H-bond and intermolecular interactions; (a) H-bond donor and acceptor meshes represented by pink and light green colours, respectively; (b) Hydrophobic pocket represented with blue and brown colours; (c) Aromatic receptor surface represented by blue (Edge) and light orange (face) colours; (d) interpolated charge receptor surface represented by blue and red colours; (e) SAS receptor surface represented by blue and light green colours, respectively; (f) ionizability receptor surface represented by blue (basic) and red (acidic) colours.

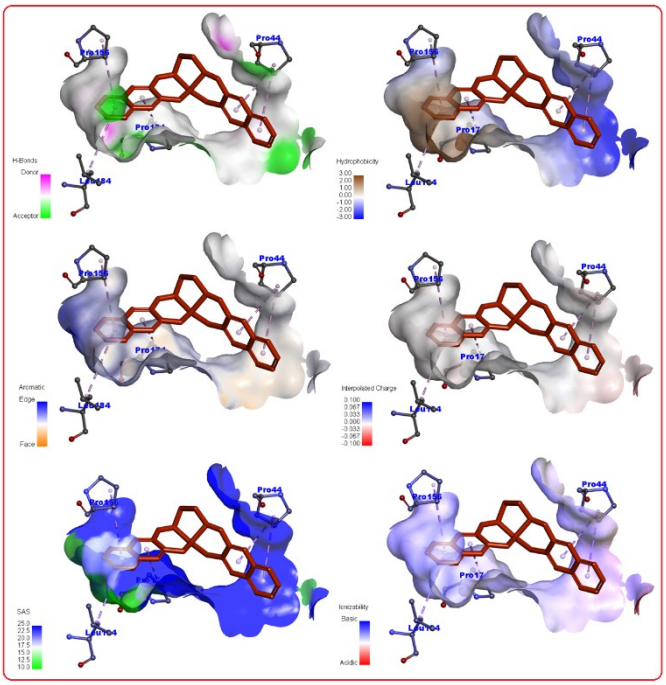

Figure S42. Graphical representation of docked Ni (II) complex (**2**) inside the SARS-CoV-2 Omicron spike protein (PDB ID: 7WK8) with its focused view for interacting residues along with H-bond and intermolecular interactions; (a) H-bond donor and acceptor meshes represented by pink and light green colours, respectively; (b) Hydrophobic pocket represented with blue and brown colours; (c) Aromatic receptor surface represented by blue (Edge) and light orange (face) colours; (d) interpolated charge receptor surface represented by blue and red colours; (e) SAS receptor surface represented by blue and light green colours, respectively; (f) ionizability receptor surface represented by blue (basic) and red (acidic) colours.

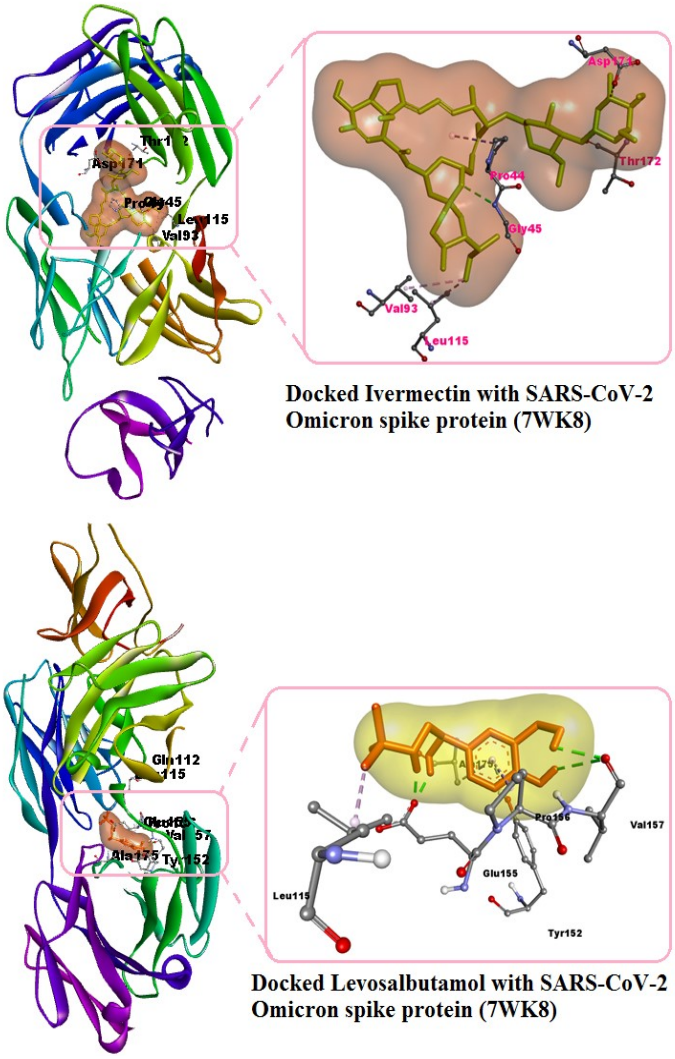

Figure S43. Graphical view of the docked ivermectin (IVM) and levosalbutamol (LVM) inside the active site of the SARS-CoV-2 Omicron spike protein (PDB ID: 7WK8) with its focussed view for interacting amino acid residues.

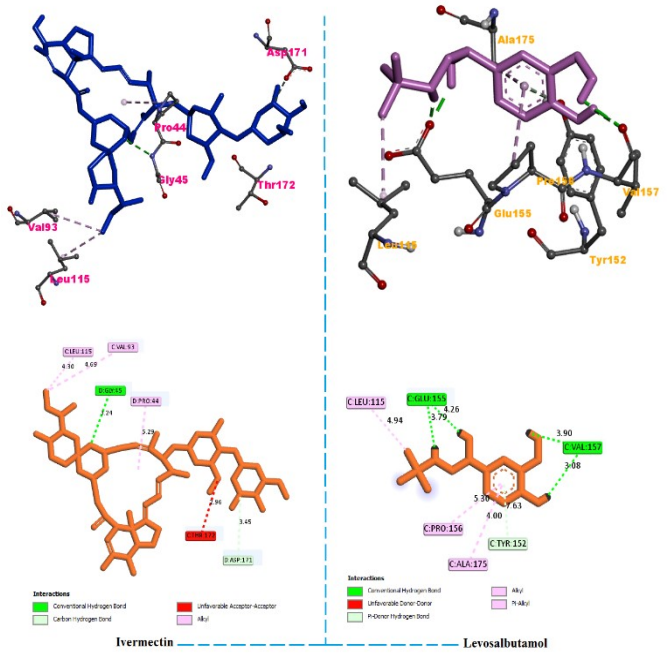

Figure S44. The top figures show 3D view of ivermectin (IVM) and levosalbutamol (LVM) with interacting residues inside the active site of the SARS-CoV-2 Omicron spike protein (PDB ID: 7WK8). The bottom figures show the 2D representation of docked ivermectin (IVM) and levosalbutamol (LVM) with types of interactions.

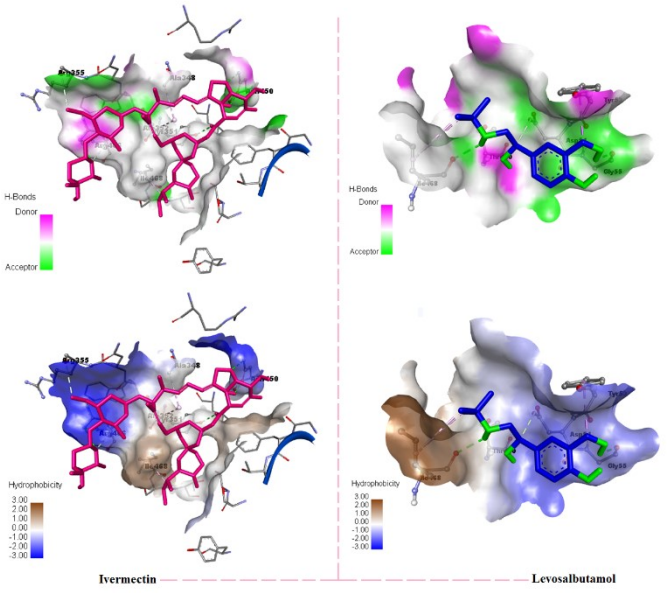

Figure S45. H-bond (top view) and hydrophobicity (bottom view) plot of interacting amino acid residues of SARS-CoV-2 spike protein (PDB ID: 7CWO) with the docked ivermectin (IVM) and levosalbutamol (LVM). Ivermectin (IVM) and levosalbutamol are displayed in pink and blue colour.

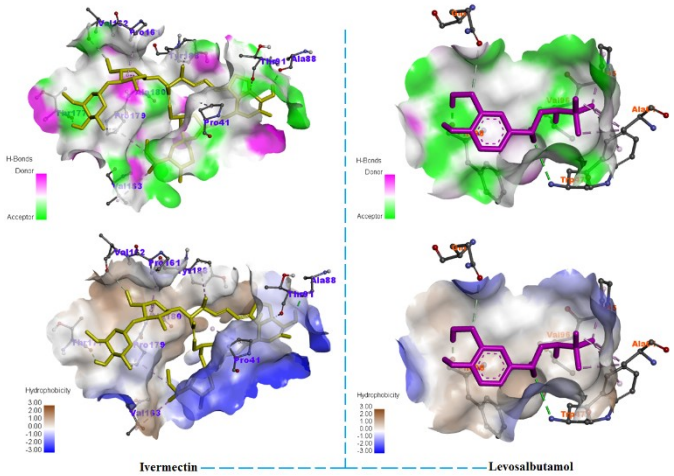

Figure S46. H-bond (top view) and hydrophobicity (bottom view) plot of interacting amino acid residues of SARS-CoV-2 Omicron spike protein (PDB ID: 7QTK) with the docked ivermectin (IVM) and levosalbutamol (LVM). Ivermectin (IVM) and levosalbutamol are displayed in yellow and pink colour.

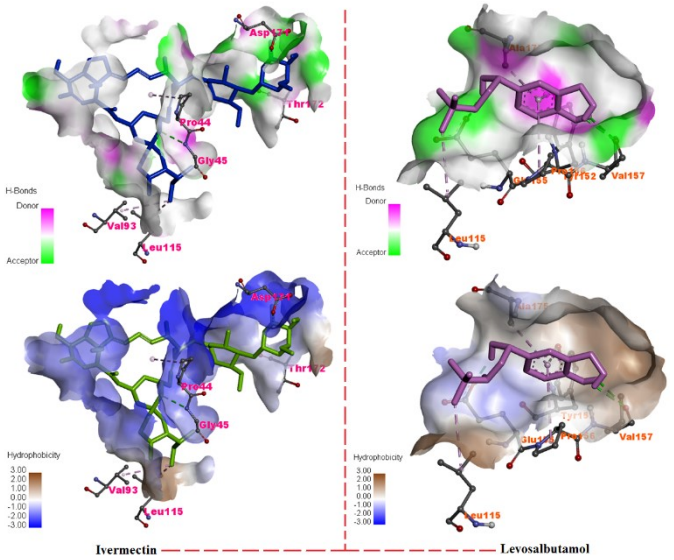

Figure S47. H-bond (top view) and hydrophobicity (bottom view) plot of interacting amino acid residues of SARS-CoV-2 Omicron spike protein (PDB ID: 7WK8) with the docked ivermectin (IVM) and levosalbutamol (LVM). Ivermectin (IVM) and levosalbutamol are displayed in blue/ purple colour and green/purple colour.

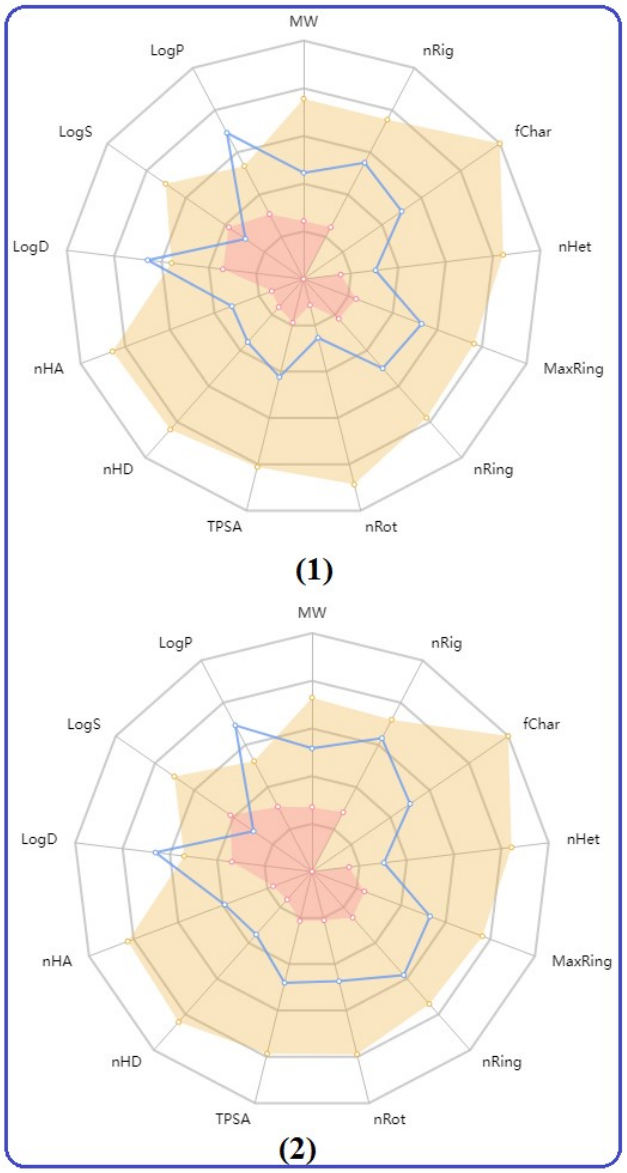

Figure S48. ADMET representation of new Schiff base Ni(II) complex (**1**) and (**2**).

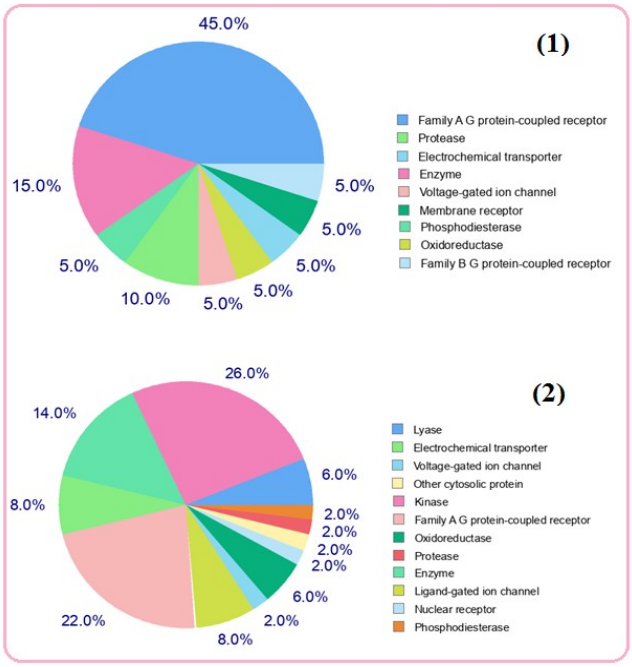

Figure S49. Pie chart representation of Swiss-target prediction for new Schiff base Ni(II) complex (**1**) and (**2**).

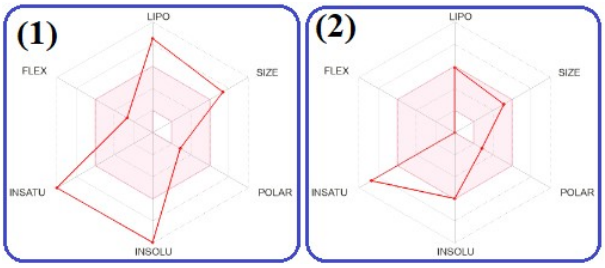

Figure S50. Graphical representation of bioavailability radar for new Schiff base Ni(II) complex (**1**) and (**2**).

Table S1. AUTODOCK parameters (docking coordinates, grid size and grid spacing) used for ivermectin (IVM) and levosalbutamol (LVM) docked with S protein from SARS CoV-2 Spike protein and the Omicron S proteins.

Autodock parameters	SARS-CoV-2 Spike protein		Omicron S proteins			
	(PDB ID:7CWO)		(PDB ID: 7QTK)		(PDB ID: 7WK8)	
	IVM	LVM	IVM	LVM	IVM	LVM
Docking coordinates (x, y, z)	65.828, 96.754, 83.245	67.703, 98.629, 85.120	90.121, 91.541, 91.147	80.231 79.562 83.762	82.232 86.624 89.258	83.752 86.358 90.712
Grid Size (x, y, z)	80.828, 111.754,9 8.245	80.828, 111.754, 98.245	92.141 89.234 93.527	87.236 88.231 87.539	79.612 73.322 82.815	81.950 87.478 85.421
Grid spacing	0.375 Å	0.375 Å	0.492 Å	0.492 Å	0.442 Å	0.442 Å

Table S2. The relevant parameters obtained from AUTODOCK outputs for ivermectin(IVM) and levosalbutamol (LVM) with SARS-CoV-2 Spike protein (PDB ID: 7CWO) and the Omicron S proteins (PDB ID: 7CQTK and 7WK8).

Property	SARS-CoV-2 Spike protein		Omicron S proteins			
	(PDB ID:7CWO)		(PDB ID: 7QTK)		(PDB ID: 7WK8)	
	IVM	LVM	IVM	LVM	IVM	LVM
Binding energy (kcal/mol)	-9.04	-5.70	-8.93	-5.68	-10.14	-5.80
Ligand efficiency	-0.15	-0.34	-0.14	-0.27	-0.16	-0.27
Inhibition constant (nM)	234.91	66.56 (μM)	284.61	65.87 (μM)	36.89	58.22 (μM)
Intermolecular Energy (kcal/mol)	-12.32	-8.08	-12.21	-8.09	-13.42	-8.16
Electrostatic energy (kcal/mol)	-0.57	-0.31	0.03	-0.78	-0.16	-1.15
Torsional energy (kcal/mol)	3.28	2.39	3.28	2.37	3.25	2.39
vdW + Hbond + desolv Energy (kcal/mol)	-11.76	-7.78	-12.24	-7.31	-13.26	-7.01
Unbound Energy (kcal/mol)	-2.80	-1.95	-3.09	-2.02	2.63	-2.06
Total energy (kcal/mol)	-2.80	-1.95	-3.09	-2.02	-2.63	-2.06

Table S3 .Pharmacokinetic Properties of the newly synthesized Ni(II) complex (**1**) and (**2**).

Property	Model Name	Predicted Value	
		(**1**)	(**2**)
Absorption	Water solubility(log mol/L)	-9.942	-6.12
	$Caco_2$ permeability(log Papp in 10^{-6} cm/s)	-4.923	-4.387
	Intestinal absorption (human) (%Absorbed)	85.919	81.246
	Skin Permeability(Log Kp)	-4.715	-3.221
	P-glycoprotein Substrate	Yes	Yes
	P-glycoprotein I inhibitor	Yes	Yes
	P-glycoprotein II inhibitor	Yes	Yes
Distribution	VDss (human) (log L/kg)	0.741	1.189
	Fraction unbound (human) (Fu)	0.665	0.809
	BBB permeability(log BB)	-2.618	-0.1488
	CNS permeability(log PS)	-0.629	-1.248
Metabolism	CYP2D6 substrate	No	No
	CYP3A4 substrate	No	Yes

	CYP1A2 substrate	Yes	Yes
	CYP2C19 inhibitor	No	Yes
	CYP2C9 inhibitor	No	Yes
	CYP2D6 inhibitor	No	No
	CYP3A4 inhibitor	No	No
Excretion	Total Clearance (log ml/min/kg)	-2.551	-0.982
	Renal OCT2 substrate	No	No
Toxicity	AMES toxicity	No	No
	Max. tolerated dose (human) (log mg/kg/day)	0.629	0.547
	hERG I inhibitor	No	No
	hERG II inhibitor	Yes	Yes
	Oral Rat Acute Toxicity (LD50) (mol/kg)	8.247	5.084
	Oral Rat Chronic Toxicity (LOAEL) (log mg/kg_bw/day)	-1.758	-2.361
	Hepatotoxicity	Yes	Yes
	Skin Sensation	No	No
	T. Pyriformis toxicity(log ug/L)	0.358	1.247
	Minnow toxicity(log Mm)	-7.441	-6.714

nviolations	2	0
nrotb	4	0
volume	515.44	354.62
LogP	10.820	5.366
Rotatable Bonds	4	0
Acceptors	2	2
Donors	0	0
Surface area	44.41	43.18

Table S4.Chemoinformatics Properties of the newly synthesized Ni(II) complex (**1**) and (**2**).

Model Name	Predicted Value	
	(**1**)	(**2**)
Molecular Formula	$C_{35}H_{25}ClNNiO_2P$	$C_{24}H_{18}N_2NiO_2$
Molecular Weight (g/mol)	616.71	425.11
GPCR ligand	-0.06	-0.02
Ion channel modulator	-0.38	-0.16
Kinase inhibitor	-0.07	-0.02
Nuclear receptor ligand	-0.15	-0.04
Protease inhibitor	-0.04	-0.05
Enzyme inhibitor	-0.14	-0.03
miLogP	7.58	4.52
TPSA	32.40	30.33
natoms	41	29
nON	3	4
nOHNH	0	0